Published December 30, 2024 as 10.3174/ajnr.A8642

REVIEW ARTICLE

Sodium MRI in Pediatric Brain Tumors

Aashim Bhatia, Cassie Kline, Peter J Madsen, Michael J Fisher, Fernando E. Boada, Timothy P.L. Roberts

ABSTRACT

Direct sodium MRI (^{23}Na-MRI) derives its signal from spin-manipulation of the ^{23}Na nucleus itself and not the more conventional and familiar ^{1}H-MRI. Although present at much lower concentrations in the human body than the ^{1}H nuclei in the water molecule H_2O, advances in coil design and pulse sequence development have enabled the feasibility of human *in-vivo* ^{23}Na-MRI. Additionally, ^{23}Na-MRI has the potential to offer nuanced physiological insights not available to conventional MRI; this forms the basis of interest in its development, and optimism for its novel clinical utility. ^{23}Na-MRI has potential to be a useful non-invasive imaging technique to assess biochemical and physiologic cellular changes in tissues, e.g. cell integrity and tissue viability. Pathologically, the concentration of *total* sodium is elevated in tumors relative to normal counterparts due to increased intracellular sodium and/or an increased proportion of extracellular space (reflecting changes in cell morphology and anomalies of homeostasis). Here we review the technological advancements with improved pulse sequences and reconstruction methods that combat the inherent challenges of measuring sodium concentrations in the pediatric brain (in particular, its short tissue T_2 value) and present detailed imaging approaches to quantifying sodium concentrations in the pediatric brain that can be assessed in various CNS pathologies, with the focus of this paper on pediatric brain tumors.

ABBREVIATIONS: ECV, extracellular volume fraction; GBCA, gadolinium-based contrast agents; ^{23}Na-MRI, sodium MRI; IBR, iterative Bowsher reconstruction; ISC, intracellular sodium concentration, TSC, total sodium concentration.

Received month day, year; accepted after revision month day, year.
From the Department of Radiology, Children's Hospital of Philadelphia, Philadelphia, PA (A.B., T.P.L.R.); Division of Oncology, Children's Hospital of Philadelphia, Philadelphia, PA (C.K., M.J.F.); Division of Neurosurgery, Children's Hospital of Philadelphia, Philadelphia, PA; Radiological Sciences Laboratory, School of Medicine, Stanford, CA (F.E.B).

Disclosure: Dr Roberts discloses remunerated roles on medical/scientific advisory boards for, or consulting positions with, Prism Clinical Imaging, Proteus Neurodynamics, Fieldline Inc. and WestCan Proton Therapy. All other authors declare no conflicts of interest related to the content of this article.

Please address correspondence to Aashim Bhatia, MD, MS, Department of Radiology, Children's Hospital of Philadelphia, 3500 Civic Center Blvd., 2nd Floor, Office #2592 Philadelphia, PA 19104, USA, aashimbhatia@gmail.com

INTRODUCTION

Direct sodium MRI (^{23}Na-MRI) derives its signal from spin-manipulation of the ^{23}Na nucleus itself and is present at much lower concentrations in the human body than the ^{1}H nuclei in the water molecule H_2O. Advances in coil design and pulse sequence development have enabled the feasibility of human *in-vivo* ^{23}Na-MRI, which has the potential to offer nuanced physiological insights not available to conventional MRI. ^{23}Na-MRI has potential to be a useful non-invasive imaging technique to assess biochemical and physiologic cellular changes in brain tumors, e.g. cell integrity and tissue viability, with the concentration of *total* sodium is elevated in tumors relative to normal counterparts due to increased intracellular sodium and/or an increased proportion of extracellular space (reflecting changes in cell morphology and anomalies of homeostasis). Here we review the technological advancements with improved pulse sequences and reconstruction methods that combat the inherent challenges of measuring sodium concentrations in the pediatric brain (in particular, its short tissue T_2 value) and present detailed imaging approaches to quantifying sodium concentrations in the pediatric brain that can be assessed in various CNS pathologies, with the focus of this paper on pediatric brain tumors.

MAIN BODY

Direct sodium MRI (^{23}Na-MRI) exploits similar atomic nuclear spin mechanisms that allow for conventional proton (1H) MRI, but derives its signal from manipulation of the ^{23}Na nucleus itself[1,2]. Although present at much lower concentrations in the human body than the ^{1}H nuclei in the water molecule H_2O, advances in coil design and pulse sequence development have enabled the feasibility of human in-vivo ^{23}Na-MRI. Sodium (^{23}Na) MRI uses the same MR scanner as conventional MRI (although it must be equipped with "heteronuclear" capability, primarily a broadband radiofrequency (RF) system, since the Larmor frequency of the ^{23}Na spins differs from that of ^{1}H protons). For the same reason a dedicated transmit/receive RF coil is required; however, these are now commercially available for use at both 3T and 7T. While conventional pulse sequences (e.g. gradient recalled echo) can often be manipulated to function at the resonance frequency of sodium - 33.8 MHz at 3T, instead of the conventional 127.1 MHz for ^{1}H, (based on the gyromagnetic ratios of sodium and

Copyright 2024 by American Society of Neuroradiology.

hydrogen), dedicated pulse sequences are often preferred and will be discussed below. Given the challenges with sensitivity, coil hardware and pulse sequence requirements, the adoption of ^{23}Na-MRI might present some initial challenges. However, it has the potential to offer nuanced physiological insights not available to conventional MRI and this forms the basis of interest in its development, and optimism for its novel clinical utility. ^{23}Na-MRI has potential to be a useful non-invasive imaging technique to assess biochemical and physiologic cellular changes in tissues, e.g. cell integrity and tissue viability[3,4]. ^{23}Na-MRI has demonstrated such potential in the pathophysiologic evaluation of acute ischemic stroke, multiple sclerosis, amyotrophic lateral sclerosis, migraines, and multiple tumor types, including tumors both within and outside of the central nervous system[3,5–11]. There is no radiation exposure with MRI (including ^{23}Na-MRI) and ^{23}Na-MRI does not use gadolinium-based contrast agents (GBCA), eliminating the potential long-term risks of these contrast agents commonly used in ^{1}H MRI; nor does it in fact rely on any other exogenous tracer (in contrast to positron emission tomography (PET) for example). The sensitivity of direct sodium imaging in *detecting* disease states stems from the tightly controlled Na+ ion homeostasis in healthy tissues which maintains a large concentration gradient between intracellular sodium concentration (ISC) at 10-15 mM and extracellular sodium at ~145 mM. The concentration of *total* sodium is elevated in tumor cells relative to normal tissues due to increased intracellular sodium concentration and/or an increased proportion of extracellular space (reflecting changes in cell morphology)[8].

In neoplastic tissue, sustained depolarization of the cell membrane with altered Na^+/H^+ pump transport kinetics precedes the high rate of mitotic activity that characterizes abnormal tumor growth leading to concomitant increase in the ISC that has been demonstrated in a number of human neoplasms (Supplemental Table 1)[12–14]. Further characterization of this rise in intracellular sodium concentration in several types of human carcinomas and glial cell lines has established a positive correlation between proliferative activity and increased intracellular Na^+:K^+ ratio (mostly due to an increase in ISC). Increase in ISC contributes to an increase in total sodium concentration (TSC). Research suggests that elevated abnormal changes in voltage-gated sodium channels ($Na_v1.3$, $Na_v1.6$) in low-grade astrocytoma and increased expression of the Na, K,-ATPase β-subunit isoforms in peri-tumoral astrocytes may contribute to the increases in both ISC and TSC[15]. In addition, pediatric brain tumor tissues consist of up to 30% non-neoplastic cells, including glioma-associated microglia, monocyte-derived macrophages, myeloid-derived suppressor cells, and tumor-infiltrating $CD4^+$ and $CD8^+$ T-cells[16]. The tumor microenvironment is similarly characterized by low glucose, low oxygen, and high acidity, resulting from aerobic glycolysis (Warburg effect) in highly proliferative cancer cells to meet their high nutrient demand, despite the presence of oxygen and fully functioning mitochondria[17,18]. Activation of other Na^+ ion transport proteins (such as H^+ extrusion protein Na^+/H^+ pump and cell volume regulatory protein Na-K-Cl pumps) could also contribute to increased ISC and TSC in tumor tissues, which have been detected in glioma cells as well as in glioma-associated microglia and peri-tumoral reactive astrocytes[19]. Changes of Na^+ transport protein expression and function in tumor cells, tumor-associated glial cells and tumor infiltrating immune cells play a role in the elevated sodium concentrations in pediatric brain tumors[20]. As such, direct sodium imaging with ^{23}Na-MRI offers attractive sensitivity to processes of the cell membrane.

There have been promising results suggesting that sodium levels are able to predict CNS tumor types and even predict progression-free survival[11,21]. ^{23}Na-MRI has been shown to be a marker of tumor proliferation in animal glioma models and, importantly, has shown the ability to distinguish between post-treatment necrosis and treatment responses[22]. In adult (human) brain tumors, ^{23}Na-MRI has demonstrated the ability to provide an additional marker for differentiating high-grade and low-grade tumors, treatment response, and even determining a molecular mutation, with direct measurement of sodium concentrations complementary to ^{1}H MRI[11,13,21]. In one study of 20 adult patients with malignant brain tumors, the mean sodium concentration (in millimoles per kilogram wet weight) was 61±8 for grey matter, 69±10 for white matter, 135±10 for cerebrospinal fluid, 113±14 for vitreous humor, and, *importantly* 103±36 for brain tumor, which is significantly elevated compared to reference brain tissues[12]. Recently, we published the first report of application of ^{23}Na-MRI to *pediatric* brain tumor imaging[13].

Technical challenges in ^{23}Na-MRI in the pediatric brain necessitate an optimized MRI sequence, for which there is currently no standard approach or consensus. This paper will summarize the multiple technical factors and hardware involved in estimating sodium concentrations using ^{23}Na-MRI in the pediatric brain, considering pulse sequences, RF coils, and reconstruction methods. In addition, incompletely appreciated physiology associated with sodium changes in the brain during myelination or even in newborns with relatively more incomplete myelination compared to older children present areas of interest in the research field as well as essential questions that need to be answered as a part of clinical implementation.

Equipment: Details of the ^{23}Na MRI technique will be dependent on the MRI system and hardware available. A brief overview of hardware requirements will be necessary before discussing the ^{23}Na-MRI technique. Sodium concentrations are 1000s of fold less than hydrogen protons in the human body, particularly in the human brain, where there is an average of 35-45 mM sodium ions compared to 80M proton concentration in the hydrogen nuclei of water molecules (Table 1)[23]. Not only is the sodium ion concentration so much lower (compromising sensitivity) but the fundamental sensitivity of the NMR experiment is intrinsically lower for the ^{23}Na nucleus compared to ^{1}H, being linearly dependent on the gyromagnetic ratio (which differs between nuclei and is approximately 25% for sodium compared to hydrogen). This compromises sensitivity (and, ultimately, signal to noise ratio, SNR) further. Worse still, the T_2 decay constants of sodium nuclei *in vivo* are very short (especially for the intracellular component – as low as ~3-5ms at 3T) which presents a further challenge to signal detection, requiring very short echo times (TE). These factors have generally led to a practical minimum field strength requirement of 3T to obtain adequate sodium signal. Additionally, because of the different Larmor frequency of sodium [approximately 33.8 MHz at 3T], the scanner will need to be equipped with a broadband radiofrequency system [sometimes called heteronuclear, or X-nucleus, package]. Since the first FDA approved 3T system in 1999, research in ^{23}Na MRI has benefited from improved gradients and electronics to improving clinical feasibility through shorter minimum TE values. Lower spatial resolution (~ 3mm isotropic) is often an accepted compromise along with relatively long acquisition times (~10 min) due to the low SNR. SNR increases approximately linearly with increased field strengths (although T_2 values may shorten further), and there are thus advantages of imaging at higher field strengths,

namely 7T, which will be discussed further below.

Imaging Technique: Total sodium concentration (TSC) within the brain is signal from both the extracellular and intracellular spaces. The extracellular space consists primarily of the interstitial space that contains extracellular matrix and cells. Vascular (3% of volume) and perivascular spaces are also included in the extracellular space, but occupy a much smaller percentage. The rapid ^{23}Na-MRI signal loss which was initially believed to be from primarily short-T_2 intracellular compartments, is now considered reflective of both interstitial and intracellular spaces. Much interest is focused on resolving the intracellular and short T2 component of the sodium signal, sometimes called the bound sodium concentration (BSC).

Acquisition Approaches in ^{23}Na-MRI: Given intracellular sodium T_2 values as short as ~3-5ms compared to relatively longer (although still short) T_2 values in the extracellular space (~25-30ms), conventional imaging sequences with relatively longer echo times (TE) will be preferentially sensitive to the extracellular, and even free-fluid, sodium signal only. Consequently, images acquired with conventional echo times >~5ms tend to have the imaging characteristics of CSF maps, with relatively weak (if any detectable) contribution from brain parenchyma.

Thus, ultra-short echo times (TE ~ 0.5 - 5ms) are required to obtain signal from the rapidly decaying signal from sodium ions in the body (especially for sodium ions in the intracellular environment). Short echo time scanning can be achieved using some gradient echo sequences; ultra-short echo time (UTE) scanning tends to employ some variant of spiral or radial scanning (with signal sampling starting at or near the center of k-space) to maximize signal sensitivity[24,25,26].

Even typically-employed radial-scanning readout results in SNR loss and inefficient sampling of k-space. Optimized approaches to sampling k-space in ^{23}Na-MRI have been developed, such as twisted projection imaging (TPI), which improves the SNR [27]. Ultra-short echo time (UTE) sequences acquire spin density weighted ^{23}Na-MRI images (note these are ^{23}Na spin density, and not "proton density"), which allows for directly estimating sodium concentrations in tissues.

There is clinical interest in sodium concentrations that are reflective of the *intra*cellular space, which can be more representative of pathological diseases in children, such as in neoplasms, demyelinating disease (multiple sclerosis), and stroke.

Several strategies have been explored to suppress the relatively hyperintense ^{23}Na-MRI signal from CSF (and also, sometimes, necrosis) to emphasize relatively lower signal contributions from brain parenchyma. Inversion recovery (IR) (based on the difference in sodium T_1 values) is an approach to attempt to suppress sodium signal from CSF; however, IR has not gained significant interest due to the low SNR and limitations with SAR due to 180° pulses[28].

So-called dual echo sodium imaging has been performed in adults and children, in which two images are acquired (potentially in the same pulse sequence) at two different (but both short) echo times, TE. The signal from these images is modeled, pixelwise, for a pool comprised of two components. A simple linear equation then allows the separation of these component pools without incurring the SNR losses associated with the inversion recovery method, provided some mathematical assumptions are made. This approach allows for a much greater SNR and lower SAR compared to IR, while still achieving ^{23}Na fluid suppression. Since the dual echo approach is essentially a subtraction technique, it is also vulnerable to differential sensitivity to magnetic susceptibility artifact, leading to erroneous elevated signal on subtraction in regions of bone-tissue or air-tissue interface, that may masquerade as fluid-suppressed tissue sodium signal[27].

To illustrate the dual echo approach with corresponding mathematics we describe a simplified model formulation (after Qian et al., 2015)[27]:

Consider a simple two compartment model, consisting of one fraction a_F in a "free" environment, characterized by T_2 decay constant T_{2F} and a second ("tissue") fraction (=1-a_F) characterized by a different T_2 decay constant, T_{2T}.

FREE: α_F, T_{2F} TISSUE (1-α_F), T_{2T}

The observed sodium signal S, for a pulse sequence with echo time TE, will be an average over the two pools (weighted by compartment volume fraction and T_2 values):

$$S = So. \{ \alpha_F . \exp(-TE/ T_{2F}) + (1-\alpha_F). \exp(-TE/ T_{2T}) \},$$

noting that T_{2F} is relatively longer and T_{2T} is shorter. So, for two imaging pulse sequences with echo times 0.5ms and 5ms respectively:

Short TE: $S(0.5) = S_0 . \{ \alpha_F . \exp(-0.5/ T_{2F}) + (1- \alpha_F) . \exp(-0.5/ T_{2T}) \}$

Long TE: $S(5.0) = S_0 . \{ \alpha_F . \exp(-5/ T_{2F}) + (1- \alpha_F) . \exp(-5/ T_{2T}) \}$

Simple Subtraction (since free component is relatively bright on both)

$S(0.5) – S(5.0) \sim S_0 . \{ (1-\alpha_F) . [\exp(-0.5/ T_{2T}) - \exp(-5/ T_{2T})] \}$

$\sim S_0 . \{ (1-\alpha_F) . [\exp(-0.5/ T_{2T}) – 0] \}$ if $T_{2T} < 5ms$

$\sim S_0 (1- \alpha_F),$ if $T_{2T} > 0.5ms,$

suggesting the so-called "short T_2 image", formed by simple subtraction, yields a signal proportional to the tissue fraction of sodium $\alpha_T = (1-\alpha_F)$.

In practice, this simple subtraction fails to completely suppress longer T_2 species, since the assumption that:

$\{ \alpha_F . \exp(-0.5/ T_{2F})\} – \{ \alpha_F . \exp(-5/ T_{2F})\} \sim 0,$

is not met exactly for realistic values of T_{2F}. Consequently, we propose a *weighted* subtraction better suited for nulling of long T_{2F} species (e.g. the fluid hyperintensities that obscure conspicuity of pathology in the in vivo brain). Consider a weighting factor, β, (where β is approximately 15%):

Weighted subtraction: "$S(0.5) – \mathbf{(1+\beta)} S(5.0)" \sim So . \{ (1-\alpha_F) . [\exp(-0.5/ T_{2T}) – (1+\beta)\exp(-5/ T_{2T})] \}$

In this case the free compartment has much reduced residual signal since the assumption,

$\{ \alpha_F . \exp(-0.5/ T_{2F})\} – (1+\beta)\{ \alpha_F . \exp(-5/ T_{2F})\} \sim 0,$

does indeed hold, and thus the weighted subtraction image (WSI) yields signal proportional to the tissue sodium fraction alone. The factor, β, needed to allow complete subtraction of the free pool signal depends on the T_2 value of that fraction (T_{2F}) and on the two chosen echo times, TE). It can be determined empirically (during post-processing) or estimated based on literature T_{2F} values. Thus, the weighted subtraction can be considered to reflect the tissue sodium fraction (weighted only by T_{2T} values). Illustrations of this methodology throughout this paper will use a β=15% as an exemplar. Note, as with all subtraction techniques, but especially with those with relatively longer acquisition times [approximately 10 minutes] misregistration of the two image sets can lead to subtraction artifact. To combat this, a pulse sequence with interleaved echo times could be created or reregistration could be facilitated with the use of sodium chloride solution fiducials analogous to the commonly used vitamin E capsules for navigation sequences.

In reality, even the cellular (non-"free") pool may itself be multicompartmental. This leads to either a higher-order multicompartmental approach or at least a hierarchical multi-step, two-compartment model, likely necessitating further image acquisitions (with different TE choices). Such multi-compartment models have been used to attempt to separate intracellular sodium from extracellular sodium concentrations. Combining fluid-suppressed IR and spin density weighted imaging has also been used to estimate the pseudo-intracellular sodium concentration and extracellular volume fraction (ECV). Such a three-compartment model has been challenged to be reliable due to disease-related fluctuations in the parameters whose values are fixed by assumption: fixed *relaxation times*, fixed *intracellular sodium concentration* and fixed *volume fractions*. Others have suggested a fourth compartment, myelin water which contains equal ratios of intracellular and extracellular sodium[29]. The further expansion of differentiating sodium signal into three or even possibly four compartments may, thus, be needed to improve the accuracy of the representation of the sodium physico-chemical micro-environment. Nonetheless, the two-compartment approach offers significant promise for ready clinical adoption. It should be noted, at this point, that alternative strategies for sodium quantification based upon triple quantum filtering (TQF) may indeed offer more precise specificity but at

the price of both signal to noise as well as analysis complexity and are considered beyond the scope of current clinical implementation.

Localized T_2* mapping schemes: T_2* measured at multiple echo times has the potential to measure sodium concentrations in different molecular environments. Localized T_2* mapping can take tremendous amount of time but if combined with optimized multi-echo readout schemes (3D MERINA), the acquisition times can be decreased[30]. Furthermore, local T_2* mapping may also provide a practical basis for improving the local image blurring associated with T_2* dependent decay of signal along the spiral (or other) k-space trajectory.

Other factors in correction of relaxation effects include echo times desired, which cannot be obtained due to hardware limitations, switching times between transmit and receive channels of the RF coil, or SAR limitations restricting the minimum pulse duration (because of its high peak B_1 amplitude, and thus RF power) and in certain tissues with very short transverse relaxation times, this leads to signal loss from T_2* relaxation. It is important to realize in the clinical setting, short TR's that do not allow for complete longitudinal relaxation (<100ms) are sometimes used. Such short TR's can lead to significant biases in the estimation of the tissue sodium concentration. If T_1 and T_2* relaxation times are known, or can be reasonably estimated, relaxation effects can be corrected by calculating the relaxation correction factors for mono and bi-exponential relaxation.

Advanced Imaging Reconstruction: There are multiple approaches to image reconstructions to decrease the rather long acquisition times of ^{23}Na-MRIs and/or improve the relatively low resolution. Radial and spiral acquisitions commonly used in ^{23}Na-MRI can take advantage of compressed sensing for iterative reconstruction. With the increasing implementation of deep learning (DL)-based reconstruction algorithms in ^{1}H-MRI, analogous optimization of ^{23}Na-MRI is to be expected. However, the greater the degree of "actual" undersampling, the greater is the possibility of inaccurate estimation of the true sodium concentrations, which has been shown in prior studies[31].

^{1}H MRI provides high-resolution, low-noise anatomical detail that can be combined with ^{23}Na-MRI. Beyond simple overlay (as in e.g. fMRI), this might best be approached with a constrained reconstruction approach. This method takes into account the possibility of losing important sodium data, where only shared data between ^{1}H and ^{23}Na-MRI are interpreted. This reconstruction approach allows for improved resolution and low noise sodium images with greater contrast between grey matter and white matter[32]. One emerging technique is the iterative Bowsher reconstruction (IBR) framework, which essentially deconvolves spatial T2-blurring using a T_2 estimate from two TE's and anatomic priors from high resolution T_1-weighted or FLAIR images (figure 1)[32]. This method is widely used in sharpening PET images and has been adapted to ^{23}Na-MRI. The proton MRI is co-registered with the ^{23}Na MRI images to confirm location of brain tumors.

Clinical Implementation Vignette: We illustrate the above concepts with a specific and detailed case example of a patient with a diffuse midline glioma (DMG) of the pons. Sodium MR Imaging Acquisition: ^{23}Na-MRI images were acquired on a 3T Siemens Scanner (Prisma, Siemens AG, Erlangen, Germany), equipped with heteronuclear capabilities; the RF coil for ^{23}Na is a dual-tuned (^{1}H-^{23}Na) head volume coil (Rapid MRI, Germany). A custom-developed pulse sequence, twisted projection imaging (TPI), is used to acquire ^{23}Na-MRI data for both total sodium (TSC) and bound sodium (BSC) imaging using a dual-TE technique (~10 min per sequence, total of ~20 min to acquire both TEs), analogous to our prior work: FOV=220mm, matrix size=64x64x64, voxel size=3.44mm (isotropic), TE_1/TE_2=0.5/5ms, TR=100ms, averages=4, and TA=10 min 38sec for each TE.

Twisted Projection Imaging (TPI) and Dual Echo-based Reconstruction: Dual echo twisted projection imaging (TPI) approach to measure "Bound" sodium concentration (BSC)**,** allows for both optimized ultra-short echo time (as low as 0.3ms) acquisition as well as a deblurred image reconstruction, based on T_2* fitting, rendering higher quality reconstructed images (with reduced T_2*-blurring). The ultrashort TE is achieved via asymmetric sampling of projection imaging with radiations from the center of the k-space along the polar and azimuthal angles. The echo time is only limited by the RF excitation pulse and associated rephasing gradient in case of slice selection. The dual-TE ^{23}Na-MRI allows suppression of the elevated "free" sodium signal within both CSF and necrotic foci, resulting in improved conspicuity of both non-neoplastic from neoplastic tissue. In the examples below (figures 2-3) we use the "115%" weighted subtraction described above to optimize free fluid sodium suppression.

^{23}Na Image reconstruction: Post-processing and Quantitative Sodium MR imaging:

We have developed a post-processing method that uses the intensity of the TE_1 to linearly calibrate using the CSF region (TSC=145 mM) and noise-only background (TSC=0 mM). Sodium images are registered to anatomical T_1-weighted, T_2-weighted or FLAIR proton images using 6 degrees of freedom rigid body transformation in medical imaging processing, analysis, and visualization (MIPAV) software (figure 4).

Imaging reconstruction methods based on similar low-resolution PET and fMRI have been applied to ^{23}Na-MRI with promising results. Incorporating anatomical prior insights from ^{1}H MRI allows anatomically guided reconstruction (AGR), for example[32]. The TPI sequence relatively widely employed offers ~3.4mm isotropic resolution, somewhat comparable to fMRI and, although justifiable in terms of its physiologic value, benefits from such anatomically enhanced reconstruction.

Possible clinical utility: Sodium MRI has the potential to be a more physiologically-specific imaging marker, compared to conventional

^{1}H MRI in determining treatment responses (figure 5). Sodium MRI is sensitive to tumor recurrence that is not visualized on conventional ^{1}H MRI[33]. Thus, ^{23}Na MRI provides an objective imaging biomarker of tumor biological activity. ^{23}Na promises to offer a pivotal imaging finding in pediatric patients with brain tumors to allow neuro-oncologists the clear indication needed to modify treatment regimens, by providing a more definitive and physiologically-interpretable imaging marker of brain tumor progression and treatment efficacy.

Future directions: High-field (7T) MRI allows for technical advances in sodium imaging in the pediatric brain. The recent FDA approved 7T Terra X magnet is equipped for heteronuclear imaging with a dual frequency ^{23}Na/^{1}H coil. 7T allows for advantages in sodium MRI such as decreasing image acquisition time, improving SNR (approx. doubling that obtained at 3T), and thus increased resolution, although noting that increasing spatial resolution by a factor of two results in a decreased SNR by a factor of eight if using a 3D isovolumetric sequence[23,34,35] Thus, the potential 7T advantages must be tailored for the specific clinical question, such as in treatment of brain tumors, where early treatment effects can be better evaluated with ^{23}Na-MRI due to improved SNR.

Multimodal T_1 weighted enhancement of sodium images: Figure 6 illustrates an interesting potential integration of ^{1}H- and ^{23}Na-MRI. In this example the ^{1}H-MRI (which is weighted by tissue T_1 values) is used not only for image overlay of the ^{23}Na-MRI, but is also used as a weighted-mask, in which the T_1-weighted ^{1}H-MRI and the subtracted tissue sodium image are multiplied to yield a new sodium map, in which free fluid (and, in particular, necrotic regions) are suppressed by the combined effects of T_1-weighted hyperintensity as well as reduced surviving signal on the dual-echo ^{23}Na-MRI weighted subtraction image. In this example, peripheral sodium signal encircling the necrotic core is clearly depicted. The eventual clinical utility of such approaches remains to be explored.

Limitations of the ^{23}Na-MRI imaging approach for estimating sodium concentrations in the pediatric brain include, but are not limited to: time of imaging, with each of the dual TE sodium sequences needing ~10 min, leading to a total acquisition time ~ 20 min, rendering data collection in children somewhat challenging without sedation. Acceleration techniques and yet-shorter TE acquisitions offer some promise for development. Generally, the much lower sodium concentrations in the brain compared to ^{1}H nuclei limit the use to at least 3T, with further studies needed to optimize (and thus realize the theoretical benefits of) implementation at higher field strengths, such as 7T. Currently, the post-processing methods discussed above make a valuable contribution towards suppression of free fluid; however, complete specificity for intracellular vs. extracellular sodium warrants further development.

In conclusion, the technological advancements with improved pulse sequences and reconstruction methods allow for combatting the challenges of measuring sodium concentrations in the pediatric brain. The sodium signal is a naturally inherent signal that doesn't require exogenous tracers or ionizing radiation, and in pediatric brain tumors is reflective of the cellular physiology of neoplastic cells in the tumor microenvironment. Here we present detailed imaging approaches to quantifying sodium concentrations in the pediatric brain that can be assessed in various CNS pathologies, with the focus on brain tumors. Future applications of ^{23}Na MRI include biopsy guidance with thresholding of the sodium concentrations to visualize potential regions of tumor with the highest mitotic activity. The major advantage of using ^{23}Na-MRI will likely be to answer the complex questions on ^{1}H MRI that arise in monitoring treatment of pediatric patients with brain tumors: is there residual or recurrent tumor, differentiating tumor progression versus treatment related changes (pseudoprogression), and in some cases at presentation, differentiating between a neoplastic process versus another mimicking pathology such as demyelinating disease.

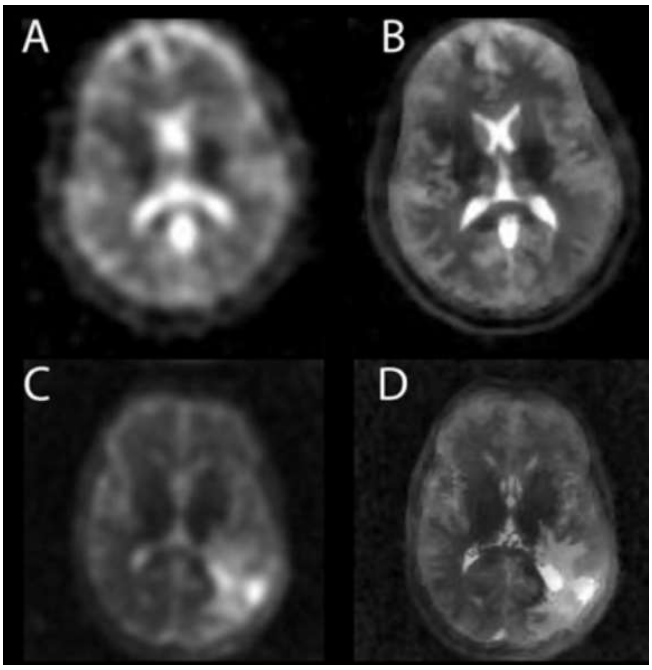

Figure 1. Deblurring ^{23}Na-MRI with iterative Bowsher reconstruction (IBR). (A) native ^{23}Na-MRI of a healthy volunteer can be significantly sharpened to (B) using two-point T_2 estimation and anatomic priors. Similarly (C) and (D) demonstrate the benefit of IBR deblurring in a glioma patient, allowing clearer intralesional resolution.

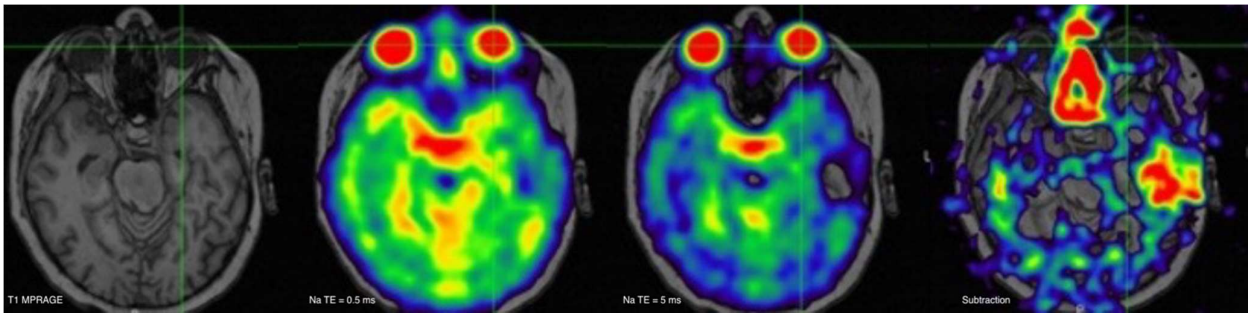

Figure 2. Dual-TE ^{23}Na-MRI in a pediatric patient with suppression of the elevated “free” sodium signal within vitreous fluid of the globe (crosshair). Note T_2 based signal loss from TE = 0.5 to 5 ms. Also note, susceptibility artifact in the left temporal lobe and nasal cavity, becoming especially pronounced on subtraction. (Same patient in figures 3-6)

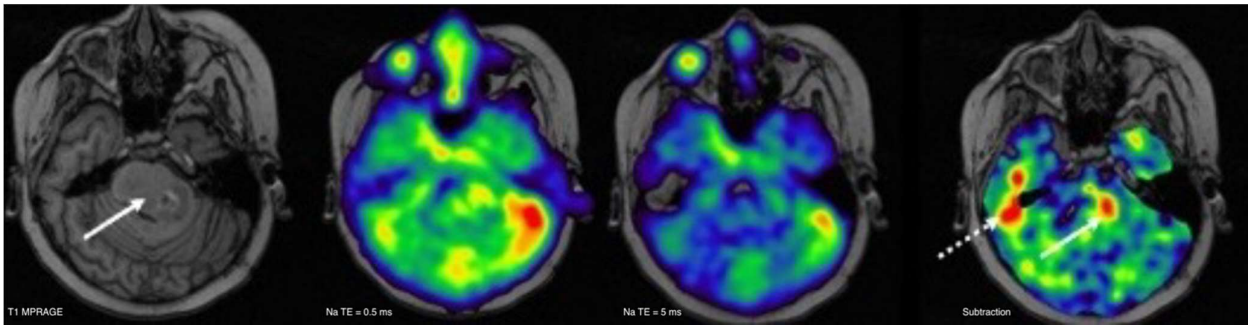

Figure 3. Diffuse midline glioma (DMG) centered in the pons in a pediatric patient. T_1 MPRAGE with tumor (solid arrow) centered in the pons extending into the left middle cerebellar peduncle. Subtraction of the two echo times demonstrates a focal region of elevated sodium in the tumor (arrow). Susceptibility artifact displays as elevated signal in the region of the right temporal bone (dashed arrow), which could potentially be misinterpreted as elevated tissue sodium concentration. (same patient as above)

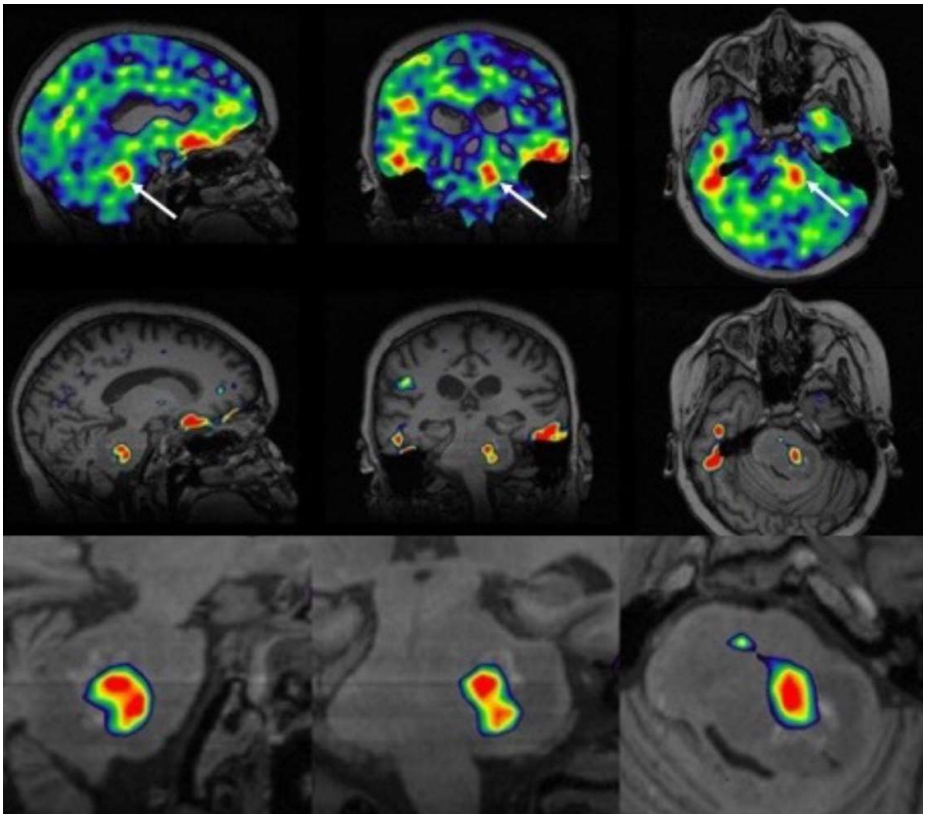

Figure 4. Thresholding the sodium concentrations in the pediatric patient above. Focal region of elevated sodium in the tumor (arrow) Thresholding allows precise depicting of the tumor.

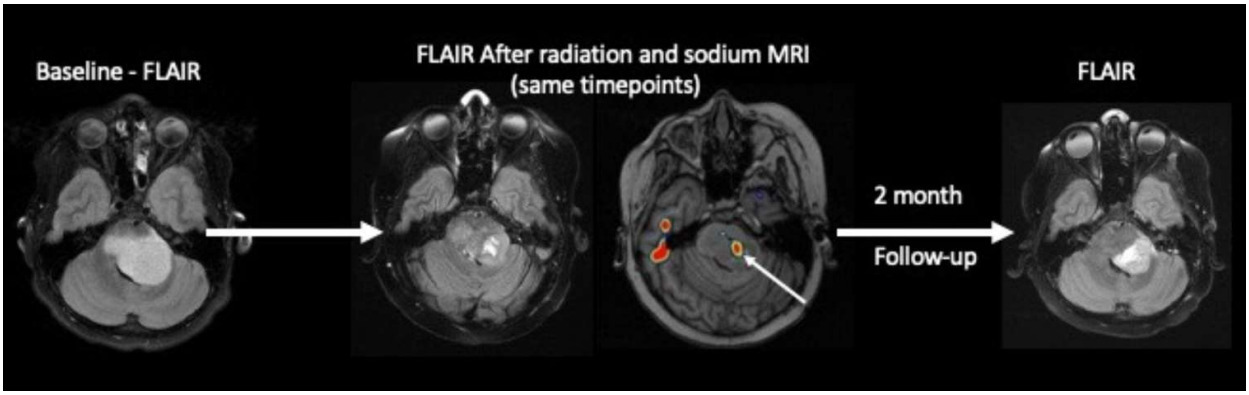

Figure 5. Pediatric DMG patient from above. The increased focus of sodium concentrations (arrow) in the tumor was acquired after radiation treatment; this region may represent: a) radioresistant region of the tumor b) region of tumor progression. Follow-up conventional MRI a further two months after radiation cessation demonstrates tumor progression in the region of the prior sodium elevation. *This anecdote supports the hypothesis that elevated sodium signal represents an early biomarker of tumor progression/recurrence.*

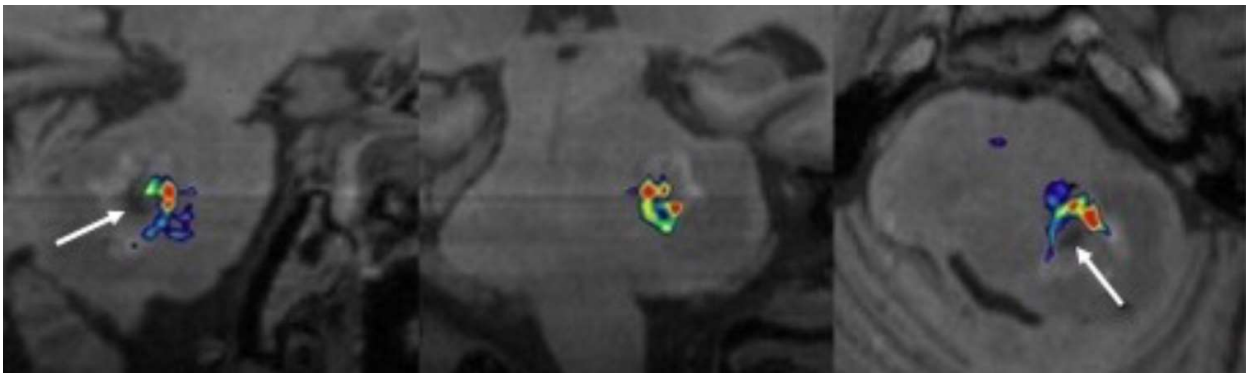

Figure 6. Using T_1 weighted sequence to further suppress necrotic regions (arrows) within the DMG (same patient as above) in a composite

^{1}H-MRI, ^{23}Na-MRI integration.

Table 1: Sensitivity of alternative nuclei in brain. Note, ^{2}D and ^{19}F are tracer techniques, as endogenous tissue concentrations are zero. Clinically, only ^{23}Na (and imaginably ^{31}P) provide sufficient in vivo sensitivity

Nucleus	Gyromagnetic Ratio MHz/T	Scanner Frequency	Tissue Concentration	Relative NMR Sensitivity	Relative Biological Sensitivity
^{1}H	42.58	127.1	88 M	1	1
^{23}Na	11.26	33.8	35-45 mM	0.092	~0.0001
^{31}P	17.24	51.7	1-10 mM	0.0663	~0.00001
^{2}D	6.54	19.5	0	0.0000096	0
^{19}F	40.08	120.24	0	0.83	0

ACKNOWLEDGMENTS

Grant Support

American Brain Tumor Association Discovery Grant

Society of Pediatric Radiology Pilot Grant

Department of Defense Exploration Grant

REFERENCES

1. Bottomley PA. Sodium MRI in man: technique and findings. In: Harris RK, ed. *Encyclopedia of Magnetic Resonance*. John Wiley & Sons, Ltd; 2007. doi:10.1002/9780470034590.emrstm1252
2. Gast LV, Platt T, Nagel AM, Gerhalter T. Recent technical developments and clinical research -applications of sodium (23Na) MRI. *Prog nucl magn reson spectrosc*. April 2023. doi:10.1016/j.pnmrs.2023.04.002
3. Deen SS, Riemer F, McLean MA, et al. Sodium MRI with 3D-cones as a measure of tumour cellularity in high grade serous ovarian cancer. *European J Radiol Open*. 2019;6:156-162. doi:10.1016/j.ejro.2019.04.001
4. Gerhalter T, Gast LV, Marty B, et al. 23 Na MRI depicts early changes in ion homeostasis in skeletal muscle tissue of patients with duchenne muscular dystrophy. *J Magn Reson Imaging*. 2019;50(4):1103-1113. doi:10.1002/jmri.26681
5. Schepkin VD. Sodium MRI of glioma in animal models at ultrahigh magnetic fields. *NMR Biomed*. 2016;29(2):175-186. doi:10.1002/nbm.3347
6. LaVerde G, Nemoto E, Jungreis CA, Tanase C, Boada FE. Serial triple quantum sodium MRI during non-human primate focal brain ischemia. *Magn Reson Med*. 2007;57(1):201-205. doi:10.1002/mrm.21087
7. Huhn K, Engelhorn T, Linker RA, Nagel AM. Potential of sodium MRI as a biomarker for neurodegeneration and neuroinflammation in multiple sclerosis. *Front Neurol*. 2019;10:84. doi:10.3389/fneur.2019.00084
8. Madelin G, Regatte RR. Biomedical applications of sodium MRI in vivo. *J Magn Reson Imaging*. 2013;38(3):511-529. doi:10.1002/jmri.24168
9. Grapperon A-M, Ridley B, Verschueren A, et al. Quantitative brain sodium MRI depicts corticospinal impairment in amyotrophic lateral sclerosis. *Radiology*. 2019;292(2):422-428. doi:10.1148/radiol.2019182276
10. Boada FE, Qian Y, Nemoto E, et al. Sodium MRI and the assessment of irreversible tissue damage during hyper-acute stroke. *Transl Stroke Res*. 2012;3(2):236-245. doi:10.1007/s12975-012-0168-7
11. Regnery S, Behl NGR, Platt T, et al. Ultra-high-field sodium MRI as biomarker for tumor extent, grade and IDH mutation status in glioma patients. *Neuroimage Clin*. 2020;28:102427. doi:10.1016/j.nicl.2020.102427
12. Ouwerkerk R, Bleich KB, Gillen JS, Pomper MG, Bottomley PA. Tissue sodium concentration in human brain tumors as measured with 23Na MR imaging. *Radiology*. 2003;227(2):529-537. doi:10.1148/radiol.2272020483
13. Bhatia A, Lee VK, Qian Y, et al. Quantitative sodium (23na) MRI in pediatric gliomas: initial experience. *Diagnostics (Basel)*. 2022;12(5). doi:10.3390/diagnostics12051223
14. Thulborn KR, Davis D, Adams H, Gindin T, Zhou J. Quantitative tissue sodium concentration mapping of the growth of focal cerebral tumors with sodium magnetic resonance imaging. *Magn Reson Med*. 1999;41(2):351-359. doi:10.1002/(sici)1522-2594(199902)41:2<351::aid-mrm20>3.0.co;2-h
15. Guan G, Zhao M, Xu X, et al. Abnormal changes in voltage-gated sodium channels subtypes NaV1.1, NaV1.2, NaV1.3, NaV1.6 and CaM/CaMKII pathway in low-grade astrocytoma. *Neurosci Lett*. 2018;674:148-155. doi:10.1016/j.neulet.2018.03.047
16. Gieryng A, Pszczolkowska D, Walentynowicz KA, Rajan WD, Kaminska B. Immune microenvironment of gliomas. *Lab Invest*. 2017;97(5):498-518. doi:10.1038/labinvest.2017.19
17. Liberti MV, Locasale JW. The warburg effect: how does it benefit cancer cells? *Trends Biochem Sci*. 2016;41(3):211-218. doi:10.1016/j.tibs.2015.12.001
18. Scharping NE, Delgoffe GM. Tumor Microenvironment Metabolism: A New Checkpoint for Anti-Tumor Immunity. *Vaccines (Basel)*. 2016;4(4). doi:10.3390/vaccines4040046
19. Cong D, Zhu W, Kuo JS, Hu S, Sun D. Ion transporters in brain tumors. *Curr Med Chem*. 2015;22(10):1171-1181. doi:10.2174/0929867322666150114151946
20. Rotoli D, Cejas M-M, Maeso M-D-C, et al. The Na, K-ATPase ß-Subunit Isoforms Expression in Glioblastoma Multiforme: Moonlighting Roles. *Int J Mol Sci*. 2017;18(11). doi:10.3390/ijms18112369
21. Biller A, Badde S, Nagel A, et al. Improved brain tumor classification by sodium MR imaging: prediction of IDH mutation status and tumor progression. *AJNR Am J Neuroradiol*. 2016;37(1):66-73. doi:10.3174/ajnr.A4493
22. Schepkin VD, Ross BD, Chenevert TL, et al. Sodium magnetic resonance imaging of chemotherapeutic response in a rat glioma. *Magn Reson Med*. 2005;53(1):85-92. doi:10.1002/mrm.20332
23. Wilferth T, Gast L, Lachner S, et al. X-Nuclei MRI on a 7T MAGNETOM Terra: Initial Experiences.

24. Du J, Bydder M, Takahashi AM, Carl M, Chung CB, Bydder GM. Short T2 contrast with three-dimensional ultrashort echo time imaging. *Magn Reson Imaging*. 2011;29(4):470-482. doi:10.1016/j.mri.2010.11.003
25. Bydder M, Ali F, Saucedo A, et al. A study of 3D radial density adapted trajectories for sodium imaging. *Magn Reson Imaging*. 2021;83:89-95. doi:10.1016/j.mri.2021.07.004
26. Feng L. Golden-Angle Radial MRI: Basics, Advances, and Applications. *J Magn Reson Imaging*. 2022;56(1):45-62. doi:10.1002/jmri.28187
27. Qian Y, Panigrahy A, Laymon CM, et al. Short-T2 imaging for quantifying concentration of sodium ((23) Na) of bi-exponential T2 relaxation. *Magn Reson Med*. 2014;74(1):162-174. doi:10.1002/mrm.25393
28. Wilferth T, Gast LV, Stobbe RW, et al. 23Na MRI of human skeletal muscle using long inversion recovery pulses. *Magn Reson Imaging*. 2019;63:280-290. doi:10.1016/j.mri.2019.08.012
29. Stobbe R, Boyd A, Smyth P, Emery D, Valdés Cabrera D, Beaulieu C. Sodium Intensity Changes Differ Between Relaxation- and Density-Weighted MRI in Multiple Sclerosis. *Front Neurol*. 2021;12:693447. doi:10.3389/fneur.2021.693447
30. Blunck Y, Josan S, Taqdees SW, et al. 3D-multi-echo radial imaging of 23 Na (3D-MERINA) for time-efficient multi-parameter tissue compartment mapping. *Magn Reson Med*. 2018;79(4):1950-1961. doi:10.1002/mrm.26848
31. Blunck Y, Kolbe SC, Moffat BA, Ordidge RJ, Cleary JO, Johnston LA. Compressed sensing effects on quantitative analysis of undersampled human brain sodium MRI. *Magn Reson Med*. 2020;83(3):1025-1033. doi:10.1002/mrm.27993
32. Schramm G, Filipovic M, Qian Y, et al. Resolution enhancement, noise suppression, and joint T2* decay estimation in dual-echo sodium-23 MR imaging using anatomically guided reconstruction. *Magn Reson Med*. 2024;91(4):1404-1418. doi:10.1002/mrm.29936
33. De Leon-Benedetti L, Narayanan S, Lee VK, Panigrahy A, Boada F, Bhatia A. The use of sodium MRI in the diagnosis of an anaplastic astrocytoma during immunotherapy: a case report. *Childs Nerv Syst*. 2024;40(3):965-967. doi:10.1007/s00381-023-06195-6
34. Qian Y, Zhao T, Zheng H, Weimer J, Boada FE. High-resolution sodium imaging of human brain at 7 T. *Magn Reson Med*. 2012;68(1):227-233. doi:10.1002/mrm.23225
35. M. Pahor, Manini and MC. High Resolution Sodium Imaging of Human Brain at 7T. *Bone*. 2008;23(1):1-7.
36. Huang L, Bai J, Zong R, et al. Sodium MRI at 7T for Early Response Evaluation of Intracranial Tumors following Stereotactic Radiotherapy Using the CyberKnife. *AJNR Am J Neuroradiol*. 2022;43(2):181-187. doi:10.3174/ajnr.A7404
37. Nunes Neto LP, Madelin G, Sood TP, et al. Quantitative sodium imaging and gliomas: a feasibility study. *Neuroradiology*. 2018;60(8):795-802. doi:10.1007/s00234-018-2041-1
38. Nagel AM, Bock M, Hartmann C, et al. The potential of relaxation-weighted sodium magnetic resonance imaging as demonstrated on brain tumors. *Invest Radiol*. 2011;46(9):539-547. doi:10.1097/RLI.0b013e31821ae918

SUPPLEMENTAL FILES

Supplemental Table 1: Sodium MRI in Human Subjects with Brain Tumors

Pathology	^{23}Na MRI Technique	Sample Size	Objective	Results	Limitation	Year/Reference
Brain tumors treated with stereotactic radiation therapy	7T Homemade birdcage coil Twisted projection imaging	n =16 12 men, 24–75 years of age	Investigate feasibility of ^{23}Na MRI at 7T for the evaluation of radiotherapeutic efficacy in brain tumors	Changes in the TSC were quantified at 7T and used to detect radiobiologic alterations in brain tumors at early time points after CyberKnife radiation therapy	Coil differences with shimming deceased performance of B0 shimming and the SNR of sodium imaging Small number of patients, and short follow-up period	2022/[36]
Treatment naïve gliomas	7T Double-resonant (^{1}H/^{23}Na) quadrature birdcage coil 3D attenuation-adapted projection reconstruction technique	n = 34 mean age, 51.29 years, WHO grades 1-4	^{23}Na MRI to reflect treatment-naïve gliomas in correlation with progression-free survival and tumor classification [isocitrate dehydrogenase (IDH)	Sodium signal was significant predictor of isocitrate dehydrogenase (IDH) mutation status (P = .001) Sodium signal of treatment-naïve brain	low sample size	2016/[21]

			mutation]	tumors was a predictor of progression (P = .003).		
Treatment naïve gliomas	3T 8-channel transmit-receive dual-tuned $^{1}H/^{23}Na$ head coil Two sequences: (1) FLORET: (2) FLORET with fluid suppression by inversion recovery (IR)	n = 8 (Age > 18 years old) WHO grade 2 (n=6), grade 3 (n=1), grade 4 (n=1)	Feasibility of using ^{23}Na MRI quantitative measurements to evaluate gliomas	Total sodium and extracellular volume fraction are increased in gliomas	Low number patients Model did not consider differences between signal contributions of short and long components of T2 relaxation present in subdivisions of the brain	2018/ [37]
Brain tumors	1.5T 16-element 23Na birdcage coil D twisted-projection imaging sequence with 1,240 projections on 22 cones in 3D k space was used with gradient strengths of up to 1.6 mT/m	n=20 (astrocytoma, n=17; oligodendroglioma, n=3) 12 men, mean age of 39 years; 8 women, mean age of 43 years	Quantify total tissue sodium concentration in human brain tumors.	^{23}Na MRI with short echo times quantified absolute tissue sodium concentration in patients with brain tumors and showed increased sodium concentration in tumors relative to normal brain	1.5T with low SNR	2003/ [12]
Brain tumors	7T Quadrature birdcage coil Density-adapted 3D radial projection reconstruction pulse sequence	n = 16 WHO grade 1-4 (n=14) metastases (n=2)	Potential of ^{23}NaR imaging for tissue characterization and putative additional benefits to ^{23}NaT imaging	^{23}NaR imaging reveals important physiological tissue characteristics different from ^{23}NaT imaging Combined use of ^{23}NaT and ^{23}NaR imaging might add valuable information for the functional in vivo characterization of brain tissue	Intrinsic signal loss in $^{23}NaR_{IR}$ than in $^{23}NaR_{SUB}$ imaging IR and consecutive long TRs, resulted in decreased resolution or prolonged acquisition time Higher SNR of the $^{23}NaR_{SUB}$ sequence was achieved at expense of a higher	2011/ [38]

					sensitivity to susceptibility artifact	
Pediatric patients with gliomas (Failed conventional treatment and on immunotherapy trial)	3T Dual-tuned (1H-23Na) head volume coil A custom-developed pulse sequence, twisted projection imaging BSC technique = two-TE technique	n = 26 Pediatric patients with gliomas median age of 12.0 years; range 4.9–23.3 years; 14 males	Feasibility of sodium MRI in measuring total sodium concentration (TSC) in both uninvolved brain tissues and three types of pediatric gliomas (DIPG, LGG, HGG) Secondary aim was to determine added value of imaging bound sodium concentration (BSC) as measured with the dual echo 23Na MRI	DIPG treated with radiotherapy demonstrated higher TSC values than the uninvolved infratentorial tissues ($p < 0.001$) Supratentorial LGG and HGG exhibited higher TSC values than the uninvolved WM and (GM ($p < 0.002$ for LGG, and $p < 0.02$ for HGG) Dual echo ^{23}Na MRI suppressed sodium signal within both CSF and necrotic foci	Small number of heterogeneously treated tumor cases, difficult to compare between the tumor-type groups	2022/[13]